ARTICLE IN PRESS

High-speed Railway xxx (xxxx) xxx-xxx

KeA1

Contents lists available at ScienceDirect

High-speed Railway

journal homepage: www.keaipublishing.com/en/journals/high-speed-railway



Research article

Compact, gain-enhanced 5G mmWave antenna with metallic ground-backed reflector for high-speed railway communication systems

Dunya Zeki Mohammed^a, Ahmed J.A. Al-Gburi^{b,*}

- ^a Department of Electronic and Communications Engineering, Gilgamesh University, Baghdad, Iraq
- ^b Center for Telecommunication Research & Innovation (CeTRI), Fakulti Teknologi Dan Kejuruteraan Elektronik Dan Komputer (FTKEK), Universiti Teknikal Malaysia Melaka (UTeM), Melaka 76100, Malaysia

ARTICLE INFO

Keywords: Millimeter-wave antenna Metallic ground backing reflector Gain enhanced 28/38 GHz Compact High-speed railway

ABSTRACT

This research presents a compact, high-gain millimeter-wave antenna tailored for reliable 5 G communication in high-speed railway environments. The proposed antenna supports dual-band operation at 28 GHz (n257/n258) and 38 GHz (n260), enabling robust Vehicle-to-Infrastructure (V2I) links required for next-generation railway systems. The radiator occupies only 12 mm \times 8 mm on a Rogers 6010LM substrate ($\epsilon_r = 10.2$, h = 0.64 mm). A Metallic Ground-Backing (MGB) reflector, positioned 9 mm behind the patch— $\lambda/4$ at 28 GHz—enhances forward radiation, suppresses back-lobes, and ensures highly directional coverage along railway tracks. The antenna achieves measured peak gains of 7.96 dBi at 28 GHz and 8.20 dBi at 38 GHz, with excellent impedance matching and stable radiation patterns under mobility scenarios. Its unique combination of compact footprint, reflector-aided gain enhancement, and stable dual-band performance under dynamic conditions distinguishes it from conventional millimeter-wave solutions, making it a strong candidate for 5G-based high-speed railway communication modules and arrays.

1. Introduction

The growth of fifth-generation (5 G) technology is accelerating demand for millimeter-wave (mmWave) antennas that are compact yet deliver high performance. Within this spectrum, the 28 and 38 GHz bands are particularly attractive because they can provide very high data rates, minimal latency, and larger network capacity [1,2]. However, designing efficient antennas for these frequencies poses challenges such as increased propagation losses, limited antenna aperture, and mutual coupling in densely packed arrays [3,4]. To address these issues, considerable research has focused on developing miniaturized antennas with high gain and directional radiation patterns. Conventional techniques to improve gain—such as array configurations and lens integration—often increase complexity, size, and fabrication cost. A more practical and space-efficient alternative involves the use of passive reflector structures to enhance antenna performance without altering the primary radiating element.

In support of next-generation 5G wireless communication systems, multiple mmWave frequency bands—most notably 28, 38, and

60 GHz—have been identified as promising candidates due to their ability to deliver ultra-high data rates and support massive device connectivity [5]. Among these, the 28 and 38 GHz bands have attracted extensive research attention, as they offer significantly improved throughput and capacity compared to the lower-frequency bands utilized in 4G systems [6]. However, despite their advantages, mmWave signals are inherently susceptible to high free-space path loss, which severely limits their effective coverage range. To counteract these propagation losses, the use of high-gain and directional antennas has emerged as a critical solution.

High-Speed Railway (HSR) communication represents a prominent use case for such high-gain antennas. Trains moving at speeds exceeding 300 km/h experience frequent handovers and rapidly varying wireless channels. In these scenarios, mmWave links suffer from high path loss and short coverage distances, especially when signals are obstructed by buildings or terrain (Fig. 1). Deploying antennas with strong directional gain ensures focused energy toward mobile relays on the train, improving signal reliability, mitigating Doppler effects, and enhancing data throughput. Such solutions are particularly vital for

Peer review under the responsibility of Beijing Jiaotong University.

E-mail addresses: ahmedjamal@ieee.org, ahmedjamal@utem.edu.my (A.J.A. Al-Gburi).

https://doi.org/10.1016/j.hspr.2025.08.004

Received 29 July 2025; Received in revised form 24 August 2025; Accepted 25 August 2025

2949-8678/© 2025 The Authors. Published by Elsevier B.V. on behalf of KeAi Communications Co. Ltd. This is an open access article under the CC BY license (http://creativecommons.org/licenses/by/4.0/).

Please cite this article as: D.Z. Mohammed and A.J.A. Al-Gburi, Compact, gain-enhanced 5G mmWave antenna with metallic ground-backed reflector for high-speed railway communication systems, High-speed Railway, https://doi.org/10.1016/j.hspr.2025.08.004

Corresponding author.

supporting onboard high-speed internet, passenger infotainment systems, and safety communications.

A variety of gain enhancement techniques have been proposed in the literature, including multi-layer substrates [8], arrays of shorting pins [9], dielectric lens structures [10], and engineered artificial materials [11,12]. While these approaches can improve antenna performance, they often lead to bulky configurations, complex power distribution networks, intricate fabrication processes, and narrow operational bandwidths.

Series-excited antenna arrays remain another focus of research for achieving elevated gain within the mmWave band [13-16]. For example, the authors in Ref. [13] introduced an eight-element dipole array measuring only 10 mm × 36.5 mm and delivered a peak gain of 10.9 dBi at 28 GHz. Nevertheless, the gain was considered modest given the relatively large array size. In another work, a series-driven radiator employing a microstrip-to-grounded Coplanar Waveguide (CPW) converter realised 10.3 dBi of gain within the 27.25-28.5 GHz band, but the design measured 22.8 mm × 67 mm—substantially large for mmWave integration [14]. Similarly, an SIW-based eight-element dipole array obtained up to 12.3 dBi gain across 21.1-27.82 GHz, though the overall footprint of 10 mm × 59 mm still posed a size limitation [15]. A four-element dipole array reported in Ref. [16] provided a broad operating band spanning 1.81-3.78 GHz with 6.78 dBi gain, but with overall dimensions of 64 mm × 105 mm, and comparatively low gain, its use in compact systems is constrained.

High-gain performance is commonly realized by increasing the antenna aperture, resulting in larger and more complex configurations. However, with the growing demand for compact and lightweight mmWave front-end modules, achieving gain enhancement in a miniaturized form factor remains a key design challenge. In recent years, Metamaterials (MTMs) have emerged as a compelling solution for gain enhancement without significantly increasing antenna size [17]. MTMs are engineered composite materials that exhibit extraordinary electromagnetic characteristics—such as negative permittivity or permeability—not found in naturally occurring substances. By integrating MTM structures into antenna designs, it is possible to manipulate the electromagnetic wavefront and enhance performance [18–20].

For instance, Ref. [18] employed a stack of seven MTM layers with six interleaved air gaps above a patch antenna, achieving a high gain of 13.6 dBi at 28 GHz. Likewise, the authors in Ref. [19] demonstrated that adding a single layer of distinct MTM elements could yield a gain of 11.59 dBi at the same frequency. However, these methods introduced increased complexity and resulted in high-profile, three-dimensional structures. To address these issues, a low-profile MTM-based dual bowtie antenna was proposed in Ref. [20], fabricated on a single-sheet Rogers PCB, achieving a gain of 12.2 dBi at 29 GHz while maintaining a compact and planar geometry suitable for mmWave integration.

The mmWave 5 G front-ends demand antennas that are compact, dual-band, and capable of delivering high directional gain despite the inherently low aperture efficiency of small radiators. Existing solutions, such as multilayer stacks, metasurface-loaded patches, and large arrays, often increase fabrication complexity, thickness, and cost, limiting their practicality for railway integration. To overcome these challenges, this work introduces a low-profile 12 mm × 8 mm printed antenna integrated with a Metallic Ground-Backing (MGB) reflector. Unlike conventional reflector-assisted or array-based designs, the proposed configuration achieves dual-band operation (28/ 38 GHz), reflector-aided gain enhancement, and stable performance under mobility, all within a compact single-layer structure. The reflector not only boosts forward gain but also suppresses back radiation, ensuring directional coverage along railway tracks-a critical requirement for maintaining reliable V2I links in high-speed railway scenarios. These features establish the proposed antenna as a lightweight, low-cost alternative to bulky mmWave solutions, addressing both miniaturization and performance demands of next-generation 5 G railway systems.

2. Millimeter-wave antenna design procedure

2.1. Millimeter -wave printed antenna layout alone

The antenna is designed in this study using CST Microwave Studio and implemented on a Rogers 6010LM substrate, which has a relative permittivity ($\varepsilon_{\rm r}$) of 10.2 and a thickness of 0.64 mm. The overall size of the antenna structure is compact, measuring 12 mm \times 8 mm \times 0.64 mm, making it highly suitable for integration in modern miniaturized 5G systems. The antenna geometry and detailed layout are illustrated in Fig. 2.

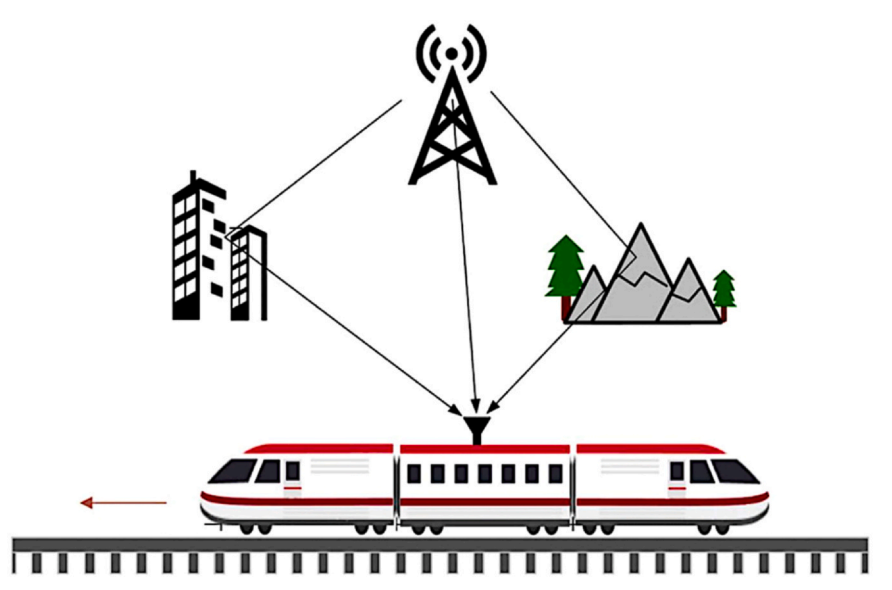


Fig. 1. 5G mmWave communication scenario for high-speed rail, showing Base Station (BS) links affected by urban and natural obstacles [7].

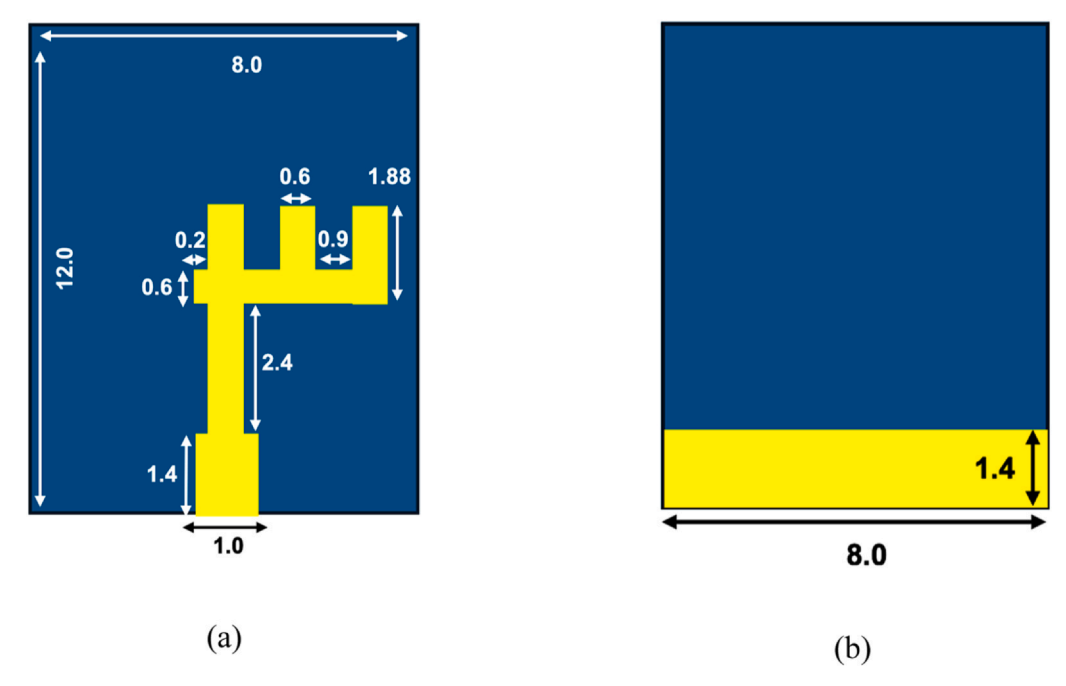


Fig. 2. Detailed layout and dimensions of the modelled mmWave antenna: (a) patch view and (b) ground view (all dimensions in millimeters).

The radiating element consists of three vertical strips of varying lengths, arranged in a fork-like configuration and connected to a central feedline. This configuration is specifically engineered to support dual-band operation at 28 and 38 GHz. The different strip lengths are responsible for generating multiple resonances, contributing to the wide operational bandwidth and stable radiation properties. The antenna ground plane is located on the opposite side of the substrate and is extended to ensure proper impedance matching and radiation control.

The antenna is excited via a standard 50-ohm SMA connector through a microstrip feedline, which is optimized for minimal reflection

and efficient energy transfer. The specific shape and dimensions of the strips were determined through parametric optimization to achieve high gain, low return loss, and desirable radiation performance at the target mmWave bands.

The antenna was developed through a five-stage evolutionary process (Fig. 3). Starting with a single vertical-strip monopole (Configuration 1), successive iterations add resonant branches that broaden the impedance bandwidth and realise dual-band operation. Configuration 2 introduces a short horizontal stub, giving a modest bandwidth extension, while Configuration 3 employs two side branches that markedly lower $|S_{11}|$ around 28 GHz. Additional parasitic elements in

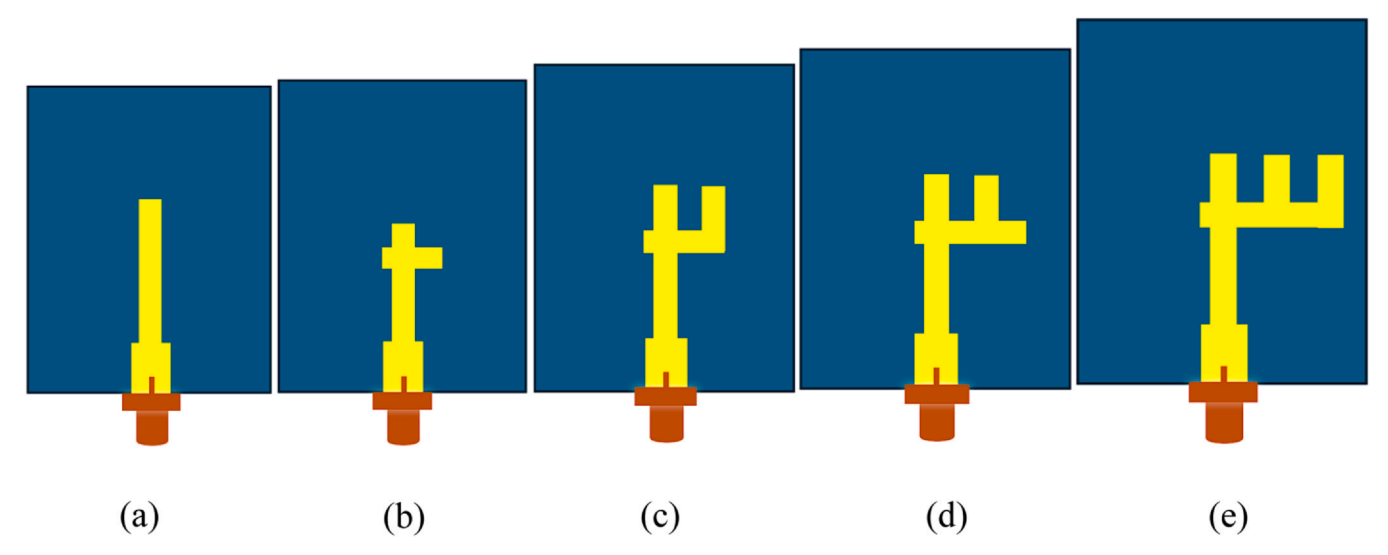


Fig. 3. Simulated reflection coefficient (IS_{11}) responses for the five configurations. Progressive branching steadily enhances impedance matching, with the final design (Configuration 5) achieving deep nulls of $-36 \, \mathrm{dB}$ at $28 \, \mathrm{GHz}$ and $-31 \, \mathrm{dB}$ at $38 \, \mathrm{GHz}$.

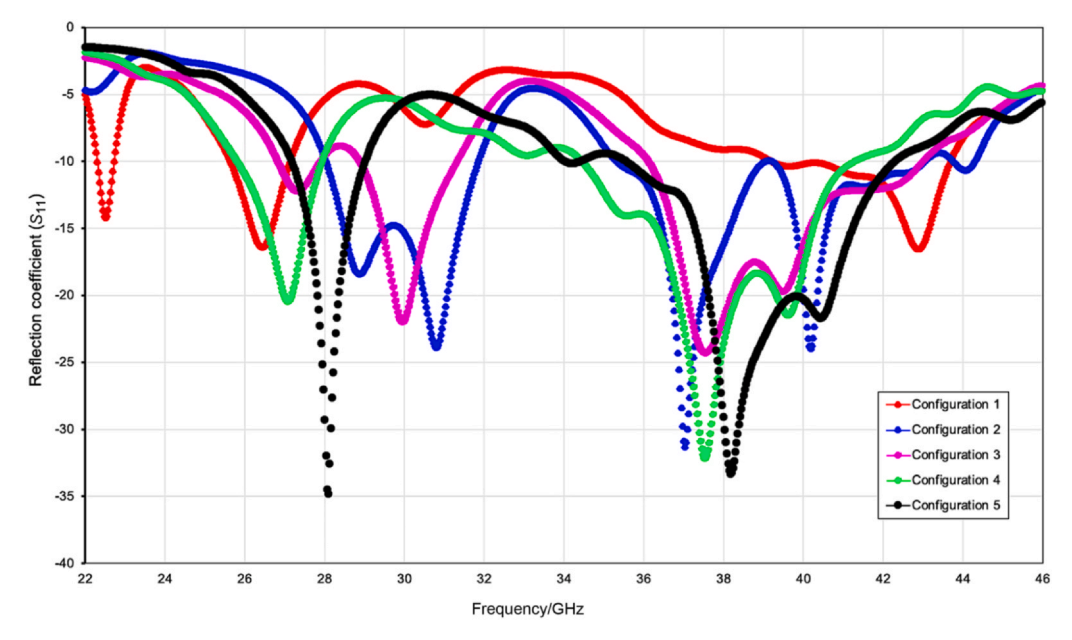


Fig. 4. Predicted S_{11} results for the five antenna configurations. Progressive design steps enhance impedance matching and bandwidth, with Configuration 5 achieving deep dual-band resonances.

Configurations 4 and 5 create well-defined resonances at both 28 and 38 GHz. Simulated $|S_{11}|$ curves in Fig. 4 confirm the benefit of each modification: every step deepens the reflection-coefficient nulls, and the final design (Configuration 5) achieves minima of $-36\,\mathrm{dB}$ at 28 GHz and $-31\,\mathrm{dB}$ at 38 GHz. This multi-branch topology therefore combines a compact 12 mm \times 8 mm footprint with wide impedance bandwidth and the high performance demanded by 5 G mmWave systems.

To better illustrate the design evolution, Table 1 summarizes each configuration and its corresponding impact on antenna performance. The table shows how successive modifications—including the addition of stubs, side branches, and parasitic elements—progressively enhance impedance matching and bandwidth, leading to the final optimized fork-like multi-branch design that supports dual-band operation at 28 and 38 GHz.

2.2. Metallic ground backing reflector design and integration

In this section, a compact MGB reflector is designed and combined with the designed antenna to improve its radiation characteristics. The MGB is realized as a planar metallic sheet with dimensions of 24 mm \times 16 mm (width $W\times$ length L), as illustrated in Fig. 5. This size remains compact compared to traditional reflector-based solutions. The main antenna, measuring 12 mm \times 8 mm \times 0.64 mm, is placed in front of the MGB reflector at a precisely controlled distance to optimize its performance. The goal of the MGB integration is to suppress backward radiation and enhance forward-directed gain by leveraging constructive interference.

To determine the optimal spacing, a comprehensive investigative analysis was carried out by adjusting the separation between the antenna and the MGB reflector. As illustrated conceptually in the figure, when the spacing equals approximately one-fourth of the

wavelength ($\lambda/4$) at 28 GHz—i.e., 9 mm—the bounced signal combines in alignment with the directly radiated signal at boresight. This condition maximizes the forward radiation, leading to substantial gain enhancement while maintaining good impedance matching across the 28 and 38 GHz frequency ranges. Despite this additional metal layer, the overall structure remains compact and suitable for integration into high-performance mmWave 5 G systems

From a theoretical perspective, the integration of a MGB reflector behind the antenna element is based on the principle of constructive interference between the direct and reflected waves in the boresight direction. When the reflector is placed at a distance $d=\frac{\lambda}{4}$ from the antenna, the reflected wave undergoes a phase shift of $\pi\pi$ due to reflection from the Perfect Electric Conductor (PEC) surface. Simultaneously, the path delay introduces another phase shift of $\beta d=\frac{2\pi d}{\lambda}=\frac{\pi}{2}$, resulting in a total phase difference of π , which inverts the reflected wave's phase.

Fig. 6(a) demonstrates how varying the air gap (d) between the radiator and the (MGB) reflector dictates both impedance match and forward gain. When the reflector is placed just 3 mm behind the patch, strong capacitive loading detunes the element: the 28 GHz resonance shifts upward, the 38 GHz null becomes shallow, and the worst-case $|S_{11}|$ hovers around -18 dB. Increasing the spacing to 6 mm eases this loading and begins to recover the 28 GHz dip, yet the higher-band match remains mediocre. Optimum behaviour emerges at d=9 mm—the $\lambda/4$ distance at 28 GHz—where the backward wave travels an extra $\lambda/2$ round trip and rejoins the direct wave in-phase. This produces textbook dual-band matching, with simulated minima of about -39 dB at 28 GHz and -31 dB at 38 GHz. Beyond this sweet spot, gaps of 12 and 15 mm let the reflected field arrive increasingly out-of-phase, so the resonances weaken and the impedance trace becomes uneven.

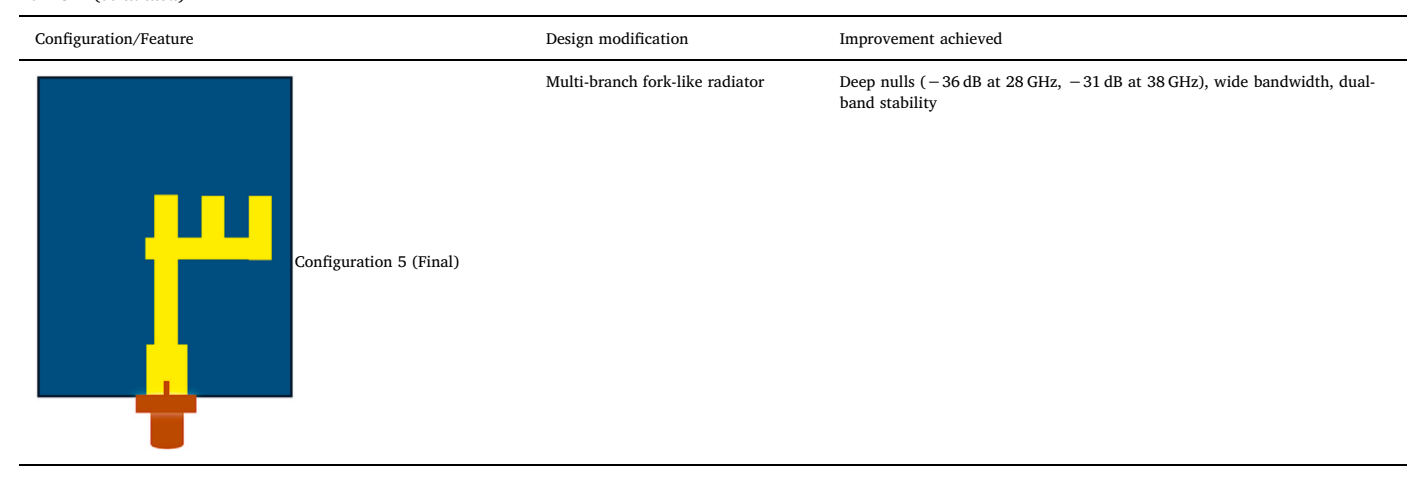
 Table 1

 Design evolution of the proposed antenna and performance improvements.

Configuration/Feature	Design modification	Improvement achieved
Configuration 1	Single vertical strip monopole	Basic resonance, narrow bandwidth
Configuration 2	Added short horizontal stub	Extended bandwidth, modest \mathcal{S}_{11} improvement
Configuration 3	Added two side branches	Stronger resonance at 28 GHz, lower
Configuration 4	Added parasitic element	Dual-band resonance begins to form

(continued on next page)

Table 1 (continued)



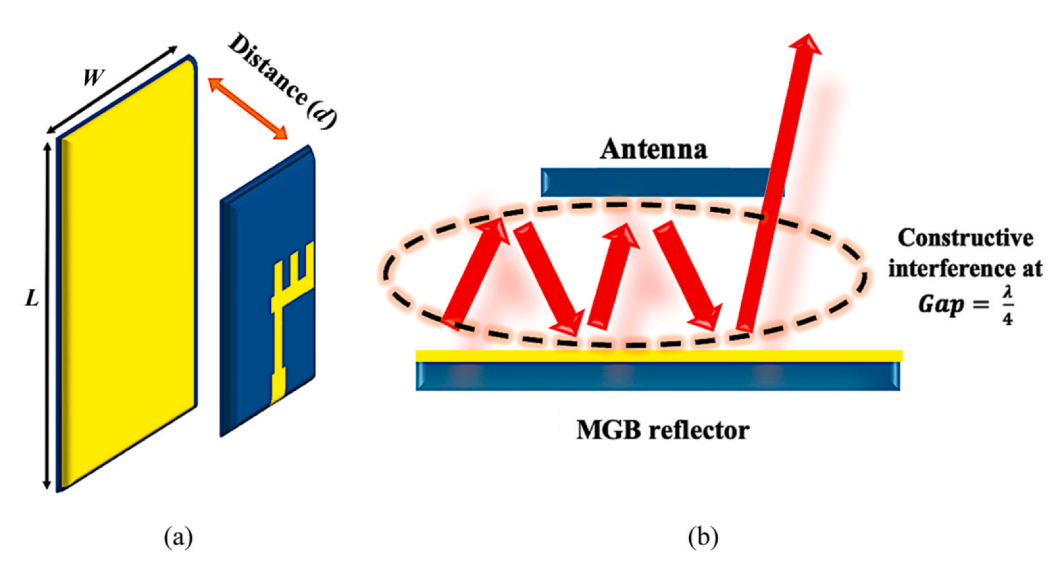


Fig. 5. Conceptual illustration of the MGB reflector and constructive interference principle. (a) Antenna–reflector layout with a $\lambda/4$ gap. (b) Field interaction showing in-phase reflections that enhance forward radiation and antenna gain.

The gain curves in Fig. 6(b) mirror these trends. At the sub-optimal 3 and 6 mm separations, phase misalignment limits constructive interference, and broadside gain stays near 7 dBi. Precisely at 9 mm, however, the in-phase addition of direct and reflected waves lifts the forward gain to roughly 8 dBi at 28 GHz and up to 10 dBi around 34–36 GHz, before settling at about 9 dBi in the 38 GHz band—equivalent to ≈ 2 dB and ≈ 3.5 dB improvements over the stand-alone radiator at 28 and 38 GHz, respectively. As the gap grows to 12 and 15 mm, constructive overlap degrades, causing both gain and pattern stability to fall off. Collectively, these results validate the analytical prediction that a $\lambda/4$ air gap maximises constructive interference, delivering the best compromise between deep dual-band impedance nulls and enhanced forward gain for mmWave 5 G front-end applications.

From a theoretical standpoint, the integration of a MGB reflector behind the radiating element enhances forward gain by utilizing the

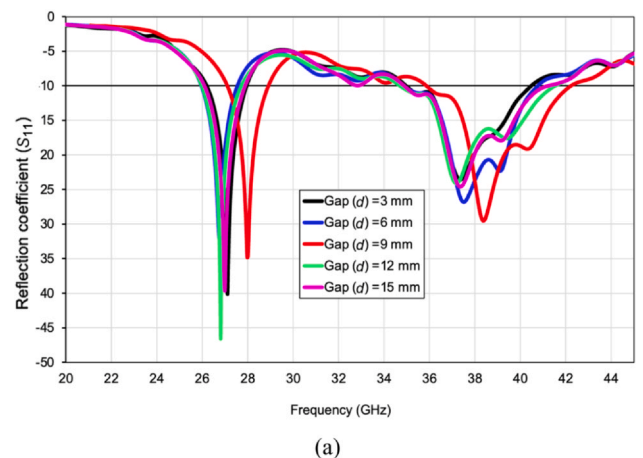
principle of constructive field superposition. When the MGB reflector is located at a distance $d=\frac{\lambda}{4}$ from the antenna, the backward-propagating wave reflects off the metallic surface, experiencing a phase inversion of $\pi\pi$ due to the PEC-like reflection property of the metal. Simultaneously, the path delay between the antenna and the reflector introduces a propagation phase shift of $\beta d=\frac{2\pi d}{\lambda}=\frac{\pi}{2}$, leading to a total phase difference of π . As a result, the reflected wave arrives at the boresight direction ($\theta=0^\circ$) in phase with the direct wave, producing constructive interference.

This can be modeled as

$$E_{\text{total}} = E_{\text{direct}} + E_{\text{reflected}} = E_0 + (-E_0 \cdot e^{-j2\beta d})$$
 (1)

At
$$d = \frac{\lambda}{4}$$
, we have

$$E_{\text{reflected}} = -E_0 \cdot e^{-j\pi} = -E_0 \to E_{\text{total}} = E_0 + E_0 = 2E_0$$
 (2)



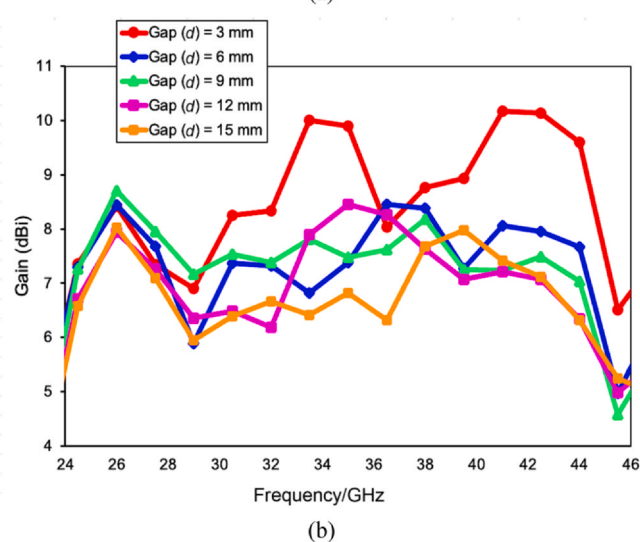


Fig. 6. Influence of antenna–MGB spacing (3–15 mm) on performance: (a) simulated $|S_{11}|$ and (b) realised gain. The 9 mm gap ($\lambda/4$ at 28 GHz) provides the strongest matching and highest forward gain.

Hence, the power gain becomes

$$G \propto |E_{\text{total}}|^2 = |2E_0|^2 = 4E_0^2$$
 (3)

This corresponds to a 6 dBi gain enhancement (i.e., a 4 times increase in radiated power) compared to an omnidirectional radiator without the MGB reflector.

For more generalized estimation, the gain of an antenna enhanced by an MGB reflector can be approximated by [21]:

$$G_{\rm MGB} \approx G_0 \left(1 + \cos \left(\frac{4\pi d}{\lambda} + \phi_{\rm r} \right) \right)$$
 (4)

where

 G_0 is the gain of the standalone antenna (without the reflector), and $\phi_r \approx \pi$ is the phase shift upon reflection from the MGB surface.

At the optimal spacing $d = \frac{\lambda}{4}$, the equation becomes

$$G_{\text{MGB}}^{\text{max}} = 2G_0 \tag{5}$$

This theoretical result supports the simulation and measurement outcomes observed in this study, confirming that the MGB reflector enhances antenna gain through directional redirection, not through multiple reflections as in resonant PRS structures. The proposed design maintains high gain while preserving compactness, making it ideal for 5G mmWave applications.

3. Fabrication and measurement results

The mmWave printed antenna integrated with the MGB reflector has been successfully fabricated and experimentally validated at this stage. To preserve the compactness of the design, Rogers 6010LM substrate was employed due to its high relative permittivity (ε_r) of 10.2 and low profile with a thickness of 0.64 mm, ensuring enhanced performance. A plastic spacer measuring approximately 9 mm was used to maintain the optimal separation between the antenna and the MGB reflector, which corresponds to a quarter-wavelength $d=\frac{\lambda}{4}$ at 28 GHz. This configuration is intended to achieve constructive interference and maximize forward gain. The fabricated prototype, including the standalone antenna, reflector, and the assembled structure, is illustrated in Fig. 7.

At mmWave frequencies, fabrication tolerances and assembly accuracy can noticeably affect antenna performance. In the proposed design, two aspects were considered: the radiator geometry and the reflector spacing. First, the fork-like radiator strips were optimized such that minor etching deviations of \pm 0.05 mm result in less than 0.2 GHz shift in resonance, keeping the antenna well within the 28 and 38 GHz target bands. Second, the metallic ground-backed reflector was placed at $\lambda/4$ (9 mm) behind the radiator. Parametric sweeps confirmed that variations of \pm 0.2 mm in the spacing only change the realized gain by less than 0.3 dB, demonstrating robustness to typical mechanical assembly tolerances. Furthermore, lateral misalignments of up to ± 0.3 mm between the radiator and reflector do not degrade the frontto-back ratio by more than 1 dB. These results confirm that the proposed design is tolerant to common PCB fabrication errors and mounting inaccuracies, making it practical for integration in 5 G highspeed railway systems.

The reflection coefficient ($|S_{11}|$) of the antenna integrated with the MGB reflector was measured using a high-frequency handheld vector network analyzer (Keysight N9951A), operating from 300 kHz to 44 GHz. Fig. 8 presents both the predicted and measured $|S_{11}|$ results of the suggested antenna structure. The predicted (CST design) curve is plotted in dashed red, while the measured response is realized in solid black.

Comparative gain and efficiency curves (Fig. 9) reveal that appending the MGB reflector raises broadside realised gain by roughly 2 dBi at 28 GHz and 3.5 dBi at 38 GHz, while the simulated and measured traces stay within about 0.5 dBi—evidence that the electromagnetic model faithfully captures connector and fixture parasitics. Across the entire 24–46 GHz span, the reflector never pulls gain below the standalone radiator; instead, it flattens the profile so that realised gain

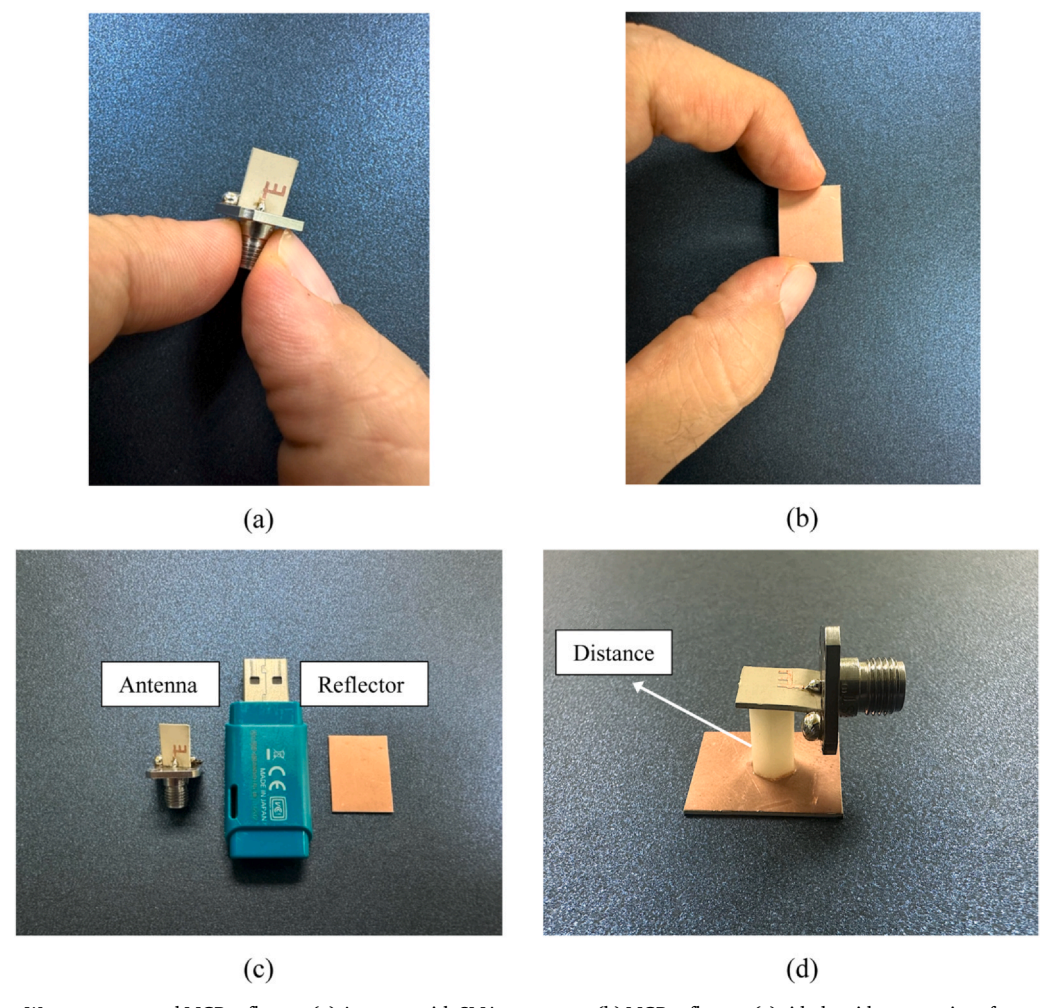
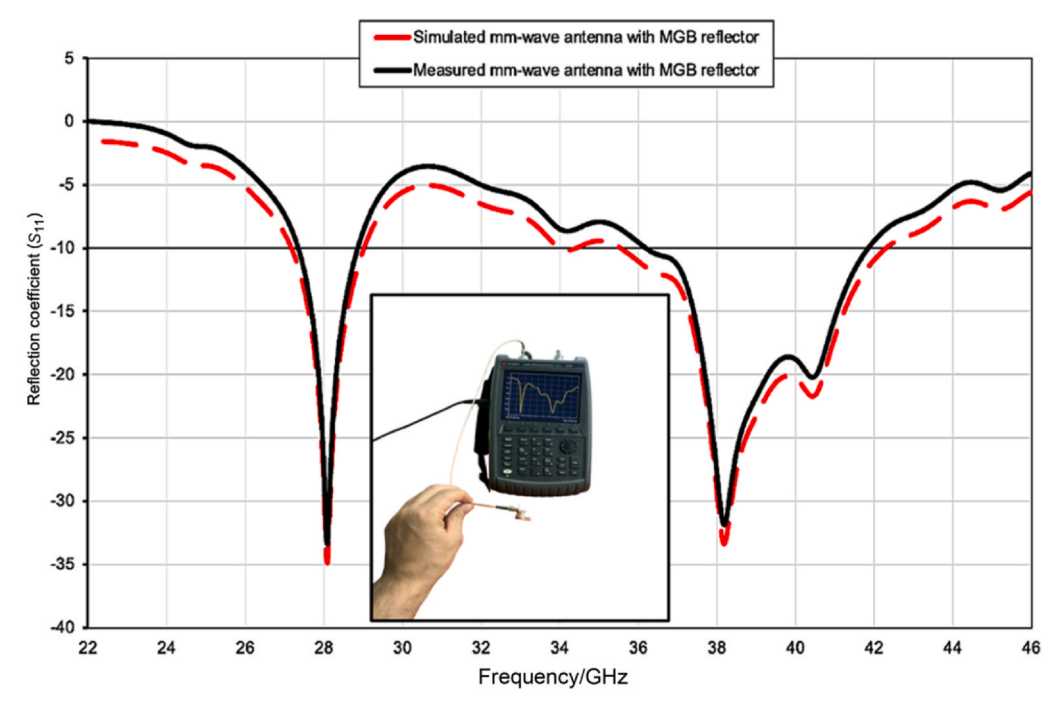


Fig. 7. Fabricated mmWave antenna and MGB reflector. (a) Antenna with SMA connector, (b) MGB reflector, (c) side-by-side comparison for scale, and (d) integrated antenna–reflector setup showing separation distance.



 $\textbf{Fig. 8.} \ \ \textbf{Simulated} \ \ \textbf{and} \ \ \textbf{measured} \ \ \textbf{reflection} \ \ \textbf{coefficient} \ \ (|S_{11}|) \ \ \textbf{of the proposed mmWave} \ \ \textbf{antenna} \ \ \textbf{with} \ \ \textbf{MGB} \ \ \textbf{reflector}.$

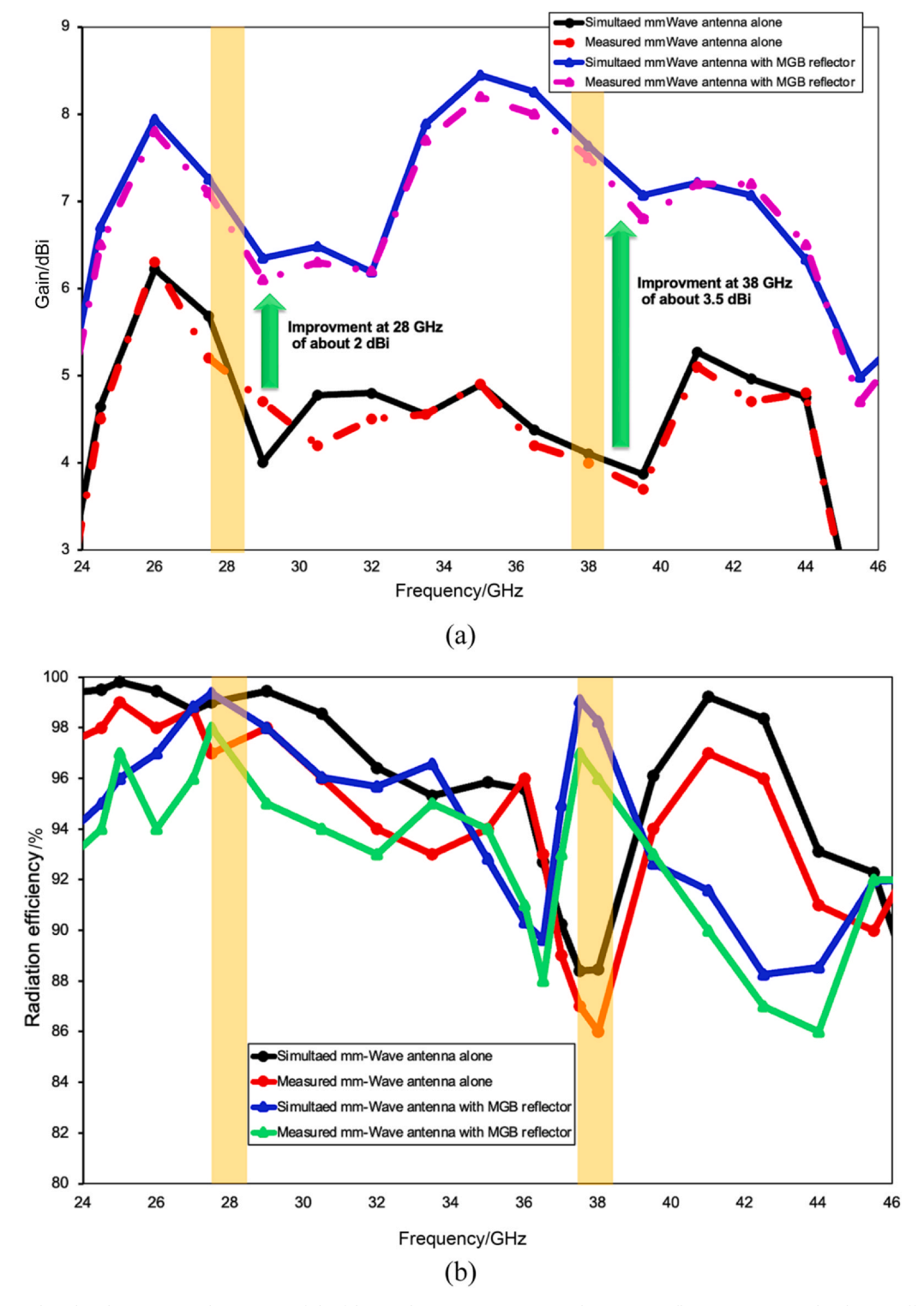


Fig. 9. Predicted and exterminated outcomes of the fabricated mmWave antenna with an MGB reflector: (a) gain and radiation efficiency.

remains above 7 dBi throughout the two highlighted $5\,\text{G/6}\,\text{G}$ service windows. Radiation efficiency likewise remains high ($\geq 90\,\%$) over most of the band: the reflector incurs only a modest 1–4 percentage-point penalty from additional surface-current loss, and the narrow dip

near 38 GHz—observed in both simulation and measurement—stems from transient destructive interference at the $\lambda/4$ spacing. These trends confirm that the MGB reflector offers a fabrication-tolerant, low-cost route to significant broadside-gain enhancement without compromising

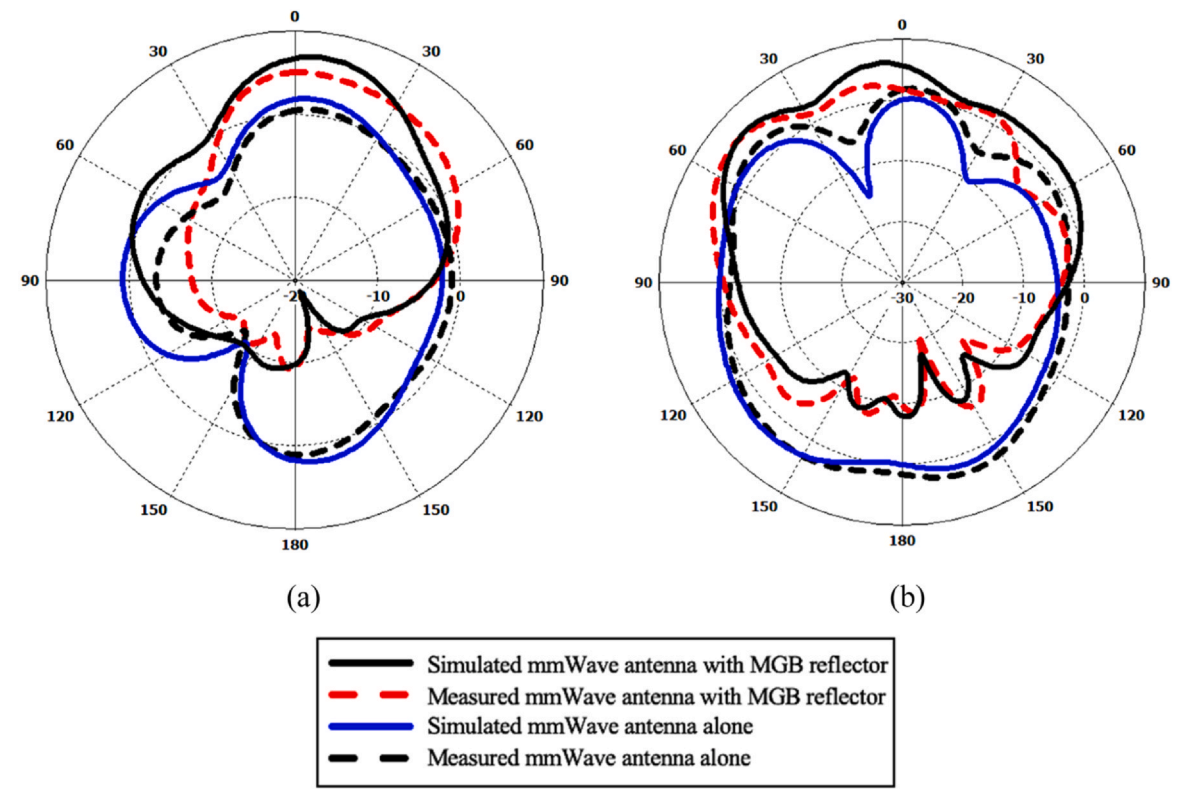


Fig. 10. Predicted and experimented E-plane ($\varphi = 90^\circ$) radiation patterns of the mmWave antenna with and without the MGB reflector: (a) 28 and (b) 38 GHz.

the efficiency thresholds demanded by FR2 cellular links and short-range radar systems.

The E-plane ($\varphi=90^\circ$) radiation patterns show that adding the MGB reflector transforms the antenna's broad cardioid beam into a sharply directive profile (Fig. 10). At 28 GHz, the stand-alone radiator presents an ~75° Half-Power Beam-Width (HPBW) and a modest ≈ 8 dB Front-to-Back Ratio (FBR); with the reflector in place, the HPBW contracts to about 55°, forward gain rises by ≈ 2 dB, and the FBR doubles to roughly 16 dB. The impact becomes even more pronounced at 38 GHz, where the beam narrows from $\approx 70^\circ$ to $\approx 45^\circ$, forward gain increases by ~ 3.5 dB, and back radiation is suppressed by more than 20 dB—yielding a highly directive pattern well suited to FR2 links. Across both bands, simulated and measured traces agree within ~ 0.5 dB, confirming that the electromagnetic model captures edge effects accurately and that the MGB reflector consistently delivers higher gain, narrower beams, and greatly improved front-to-back isolation.

Fig. 11 presents the 3D H-plane radiation patterns ($\varphi=0^\circ$) of the proposed antenna at 28 and 38 GHz with and without the MGB reflector. Without the reflector, the radiation is largely omnidirectional with strong back lobes, leading to inefficient radiation for directional communication. In contrast, the inclusion of the MGB reflector significantly enhances forward radiation, producing a strong front lobe while effectively suppressing the back lobe. This transformation from omnidirectional to highly directional patterns demonstrates the

reflector's role in improving gain and ensuring stable, focused coverage, which is critical for reliable 5 G high-speed railway communication.

To validate the advantages of the proposed antenna, a detailed comparison with related works is presented in Table 2. It can be observed that several designs achieve dual-band operation at 28/38 GHz, but often at the cost of a larger footprint [22,26] or complex reflector structures such as FSS layers [23,24]. While Al-Atyar's circular patch design [24] offers very compact dimensions, its operational bandwidth is narrow, and the radiation performance at 38 GHz is unstable. Icmez and Kurnaz [22] reported slightly higher gain at 38 GHz (8.98 dBi), but their antenna occupies a much larger area (33 mm \times 27 mm) and does not suppress back radiation. Similarly, Bhadravathi et al. [25] achieved a wide bandwidth using a double-stub monopole, but the gain remains modest (\sim 7.2 dBi) and the radiation is less directional.

By contrast, the proposed antenna offers a balanced compromise between compactness, gain, and directivity. With an overall dimension of only 24 mm \times 16 mm \times 9 mm, it achieves measured gains of 7.96 dBi at 28 GHz and 8.20 dBi at 38 GHz, while the metallic ground-backed reflector significantly enhances the forward radiation and improves the front-to-back ratio (> 16 dB at 28 GHz and > 20 dB at 38 GHz). These features are particularly beneficial for high-speed railway communication, where reliable and stable directional coverage is required under mobility.

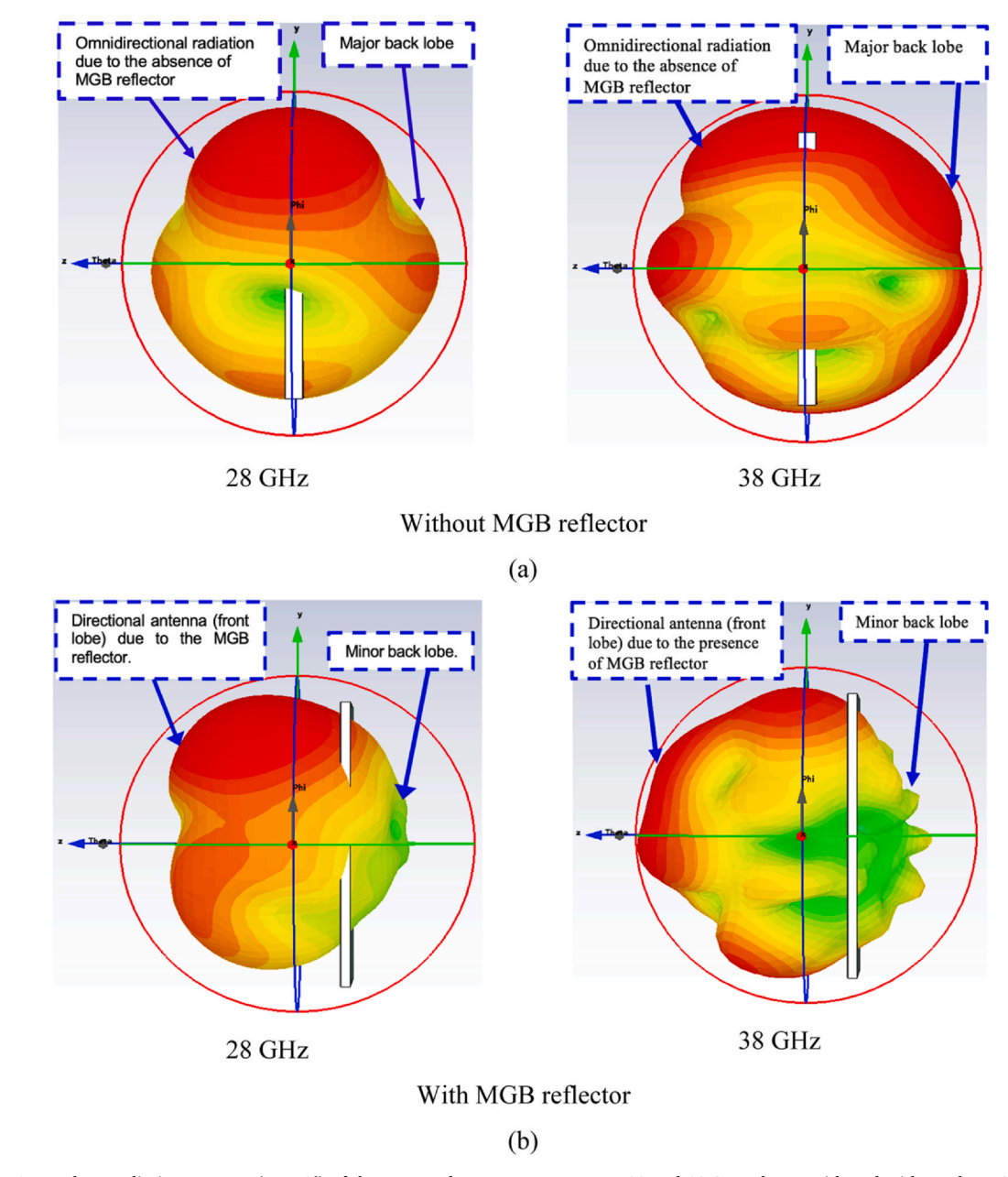


Fig. 11. 3D H-plane radiation patterns ($\varphi=0^\circ$) of the proposed mmWave antenna at 28 and 38 GHz, shown with and without the MGB reflector.

 Table 2

 Performance comparison with related works.

Ref.	Antenna type/method	Size	Bands/GHz	–10 dB BW	Peak gain/ dBi	Strengths/Weaknesses
[22]	Slot-optimized dual-band patch	33 mm × 27 mm × 1.6 mm	28, 38	1.12/1.27 GHz	7.82 at 28, 8.98 at 38	Excellent gain (esp. 38 GHz), but larger radiator area; lacks reflector/back radiation suppression.
[23]	Quad-port slot MIMO + FSS reflector	37.8 mm \times 37.8 mm \times 5.2 mm (with FSS)	25.5–30	~ 5.0 GHz	8.0 at 28 GHz	Good gain, but large FSS profile; lacks 38-GHz coverage.
[24]	FSS-backed semicircular monopole	70 mm × 70 mm × 12 mm (incl. FSS)	3.2–3.7, 5.15–5.5	0.5 each	8.0, 8.3	High gain, but sub – 6 GHz only; very large overall size.
[2]	Miniaturized end-fire dipole + ICS directors (5G-R band, sub – 6 GHz)	$0.31\lambda L \times 0.39\lambda L \times 0.008\lambda L$ ($\approx 44 \text{ mm} \times 55 \text{ mm} \times 1 \text{ mm}$ @ 2.1 GHz)	1.36-2.18 G- Hz (5G-R)	46 %	7.33 at 2.1 GHz	End-fire, wideband, railway-suited — but different band (2.1 GHz), not mmWave.
[25]	Double-stub matched monopole + slot perturbations	$0.75\lambda \times 0.66\lambda \ (\sim 8 \text{ mm} \times 7 \text{ mm at } 28 \text{ GHz equiv.})$	28, 38	27–28.75/ 36.20–42.43 GHz	7.2 at both bands	Wide BW, simple design; gain slightly lower than this work and less directional.
[26]	Crescent-shaped MIMO with slots + DGS	$60~mm \times 60~mm \times 0.508$ mm	28, 38	3.05 GHz/ 2.41 GHz	8.14 at 28, 8.04 at 38	Wide BW, but bulky, not suitable for compact integration.
This Work	Compact printed radiator + MGB reflector ($\lambda/4$, 9 mm gap)	24 mm \times 16 mm \times 9 mm (incl. gap)	28, 38	Covers n257/n258 and n260	7.96 at 28, 8.20 at 38	Low-profile, reflector-aided gain, high F/B ($> 16/20\text{dB}$), compact $12 \times 8\text{mm}^2$ radiator, stable dual-band under mobility (railway use).

D.Z. Mohammed and A.J.A. Al-Gburi High-speed Railway xxxx (xxxxx) xxxx—xxxx

4. Conclusion

This work presents a compact 12 mm × 8 mm mmWave antenna enhanced with a $\lambda/4$ -spaced MGB reflector for 5 G high-speed railway communication. The reflector significantly improves forward gain and suppresses back-lobes while keeping the design single-layer, low-profile, and cost-effective. Simulations and measurements confirm reliable dual-band operation at 28 GHz (n257/n258) and 38 GHz (n260), with stable impedance matching and directional radiation suitable for mobility scenarios. Unlike conventional high-gain mmWave solutions that rely on bulky arrays or multilayer structures, the proposed antenna achieves reflector-aided gain enhancement, compact footprint, and stable dual-band performance under high-speed conditions. These features make it particularly attractive for V2I links in high-speed rail systems, where overcoming path loss, Doppler effects, and frequent handovers is critical. With its minimal thickness, fabrication simplicity, and adaptability, the antenna is well-suited for integration into 5 G railway modules, train-mounted access points, and phased-array tiles. Future work will explore extending the MGB concept to multi-band and beam-steerable configurations, paving the way toward compact, highcapacity 6 G front ends for seamless high-speed railway connectivity.

CRediT authorship contribution statement

Ahmed J.A. Al-Gburi: Writing – review & editing, Validation, Supervision, Project administration, Investigation. **Dunya Zeki Mohammed:** Writing – original draft, Software, Methodology, Data curation, Conceptualization.

Data availability

Data will be made available on request.

Declaration of Competing Interest

The authors declare that they have no known competing financial interests or personal relationships that could have appeared to influence the work reported in this paper.

Acknowledgment

The authors would like to thank Universiti Teknikal Malaysia Melaka (UTeM) and the Ministry of Higher Education Malaysia (MOHE) for supplying the necessary materials for fabrication—such as the Rogers 6010LM substrate. We are also grateful to Universiti Teknologi Malaysia (UTM) for granting access to its mmWave measurement facilities. Finally, we acknowledge Gilgamesh University for its support with design and technical research writing.

References

[1] C.J. Meagher, S.K. Sharma, A wideband aperture-coupled microstrip patch antenna employing spaced dielectric cover for enhanced gain performance, IEEE Trans. Antennas Propag. 58 (9) (2010) 2802–2810.

- [2] Y.T. Shi, Y.L. Wu, C.H. Hu, et al., A miniaturized wideband high-gain end-fire antenna for 5G-R communication applications, High speed Railw. 2 (4) (2024)
- [3] T. Han, C. Liu Q., Li et al. Millimeter-wave high-gain substrate integrated multi-slot antenna array with a low cross polarization level, International Conference on Microwave and Millimeter Wave Technology (ICMMT), 2020, Shanghai, China, pp.
- [4] I. Tzouras, S. Koulouridis, Two-layered optimized metamaterial antenna with high gain and wide bandwidth for 5G mm-Wave applications, Int. J. Electron. Commun. 187 (2024) 155545.
- [5] R. Lu, C. Yu, Y. Zhu, et al., Millimeter-wave dual-band dual-polarized SIW cavity-fed filtenna for 5G applications, IEEE Trans. Antennas Propag. 70 (11) (2022) 10104–10112.
- [6] B.A.F. Esmail, S. Koziel, Design and optimization of metamaterial-based dual-band 28/38 GHz 5G MIMO antenna with modified ground for isolation and bandwidth improvement, IEEE Antennas Wirel. Propag. Lett. 22 (5) (2023) 1069–1073.
- [7] X.Y. Chen, W. Chen, X. Gong, et al., Wireless channel estimation for high-speed rail communications: Challenges, solutions and future directions, High speed Railw. 1 (1) (2023) 18–22.
- [8] D.C. Lugo, R.A. Ramirez, J. Wang, et al., Multilayer dielectric end-fire antenna with enhanced gain, IEEE Antennas Wirel. Propag. Lett. 17 (12) (2018) 2213–2217.
- [9] J.H. Ou, J. Huang, J. Liu, et al., High-gain circular patch antenna and array with introduction of multiple shorting pins, IEEE Trans. Antennas Propag. 68 (9) (2020) 6506–6515.
- [10] M.S. Anwar, H. Abufanas, A. Bangert, 3D printed dielectric lens for the gain enhancement of a broadband antenna, Int. J. RF Microw. Comput. Aided Eng. 30 (4) (2020) e22115.
- [11] A.J. Abdullah Al-Gburi, 5G MIMO antenna: Compact design at 28/38 GHz with metamaterial and SAR analysis for mobile phones, Prz. Elektrotech. 100 (4) (2024) 171–174
- [12] P. Danuor, J.I. Moon, Y.B. Jung, High-gain printed monopole antenna with dual-band characteristics using FSS-loading and top-hat structure, Sci. Rep. 13 (2023) 9982.
- [13] H. Wang, K.E. Kedze, I. Park, A high-gain and wideband series-fed angled printed dipole array antenna, IEEE Trans. Antennas Propag. 68 (7) (2020) 5708–5713.
- [14] N.K. Maurya, M.J. Ammann, P. Mcevoy, Series-fed omnidirectional mm-wave dipole array, IEEE Trans. Antennas Propag. 71 (2) (2023) 1330–1336.
- [15] Y. Liu, M.C.E. Yagoub, Compact omnidirectional millimeter-wave antenna array fed in series by a novel feed network, IEEE Trans. Antennas Propag. 69 (11) (2021) 7604–7612
- [16] T. Ma, J. Ai, M. Shen, et al., Design of novel broadband endfire dipole array antennas, IEEE Antennas Wirel. Propag. Lett. 16 (2017) 2935–2938.
- [17] B.A.F. Esmail, S. Koziel, S. Szczepanski, Overview of planar antenna loading metamaterials for gain performance enhancement: The two decades of progress, IEEE Access 10 (2022) 27381–27403.
- [18] Z. Wani, M.P. Abegaonkar, S.K. Koul, High-low-epsilon biaxial anisotropic lens for enhanced gain and aperture efficiency of a linearly polarized antenna, IEEE Trans. Antennas Propag. 68 (12) (2020) 8133–8138.
- [19] M. Jeong, N. Hussain, A. Abbas, et al., Performance improvement of microstrip patch antenna using a novel double-layer concentric rings metaplate for 5G millimeter wave applications, Int. J. RF Microw. Comput. Aided Eng. 31 (2) (2021) e22509.
- [20] B.A.F. Esmail, S. Koziel, Design and optimization of metamaterial-based 5G millimeter wave antenna for gain enhancement, IEEE Trans. Circuits Syst. II Exp. Briefs 70 (9) (2023) 3348–3352.
- [21] A.J.A. Al-Gburi, I.M. Ibrahim, Z. Zakaria, et al., Enhancing gain for UWB antennas using FSS: A systematic review, Mathematics 9 (2021) 3301.
- [22] B.O. Icmez, C. Kurnaz, High-gain dual-band microstrip antenna for 5G mmwave applications: Design, optimization, and experimental validation, Appl. Sci. 15 (2025) 3993.
- [23] S.M. Gaber, R.A. Kareem, A.A. Ibrahim, High isolation quad ports MIMO antenna loaded with FSS for 5G communication, Sci. Rep. 15 (2025) 20167.
- [24] S.M. Verulkar, A. Rochkari, M. Trimukhe, et al., High gain compact dual band antenna using frequency selective surface for 5G and WLAN applications, Prog. Electromagn. Res. C. 142 (2024) 1–11.
- [25] P.S. Bhadravathi Ghouse, P. Kumar, P.R. Mane, S. Pathan, T. Ali, A.-A.A. Boulogeorgos, J. Anguera, Dual-Band antenna at 28 and 38 GHz using internal stubs and slot perturbations, Technologies 12 (2024) 84, https://doi.org/10.3390/ technologies12060084.
- [26] C. Kutay, A. Nursel, O. Tayfun, et al., 28/38 GHz dual-band MIMO antenna with wideband and high gain properties for 5G applications, Int J. Electron Commun. 162 (2023) 154553.